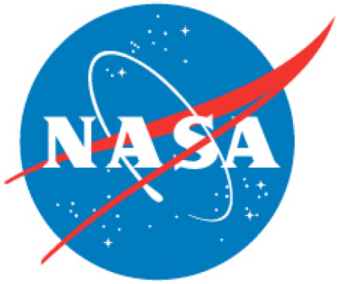

Cassini RADAR Active Rings Processing and Calibration Activities

R. West, M. Janssen, Z. Zhang, J. Cuzzi*, Y. Anderson, G. Hamilton, C. Elachi
Jet Propulsion Laboratory, California Institute of Technology, Pasadena, CA
*NASA Ames Research Center, Moffet Field, CA

October 22, 2018

Outline

- Science Motivation
- Observing geometry during radar ring scans
- Real Aperture Processing and Scaling
- Real Aperture Calibrated backscatter
- Range Compression
- Range Compressed Preliminary backscatter
- Absolute Calibration Validation using Earth Flyby Measurements

Science Motivation

- 2.2 cm wavelength radar pulses deeply penetrate icy ring particles
  - Sensitive to dielectric composition including porosity and rock vs ice mixing fraction
- Radar provides high radial resolution (potentially km-scale resolution)
  - Resolves dynamic structure such as density waves
  - Provides high resolution constraints on composition and structure

Observing Geometry

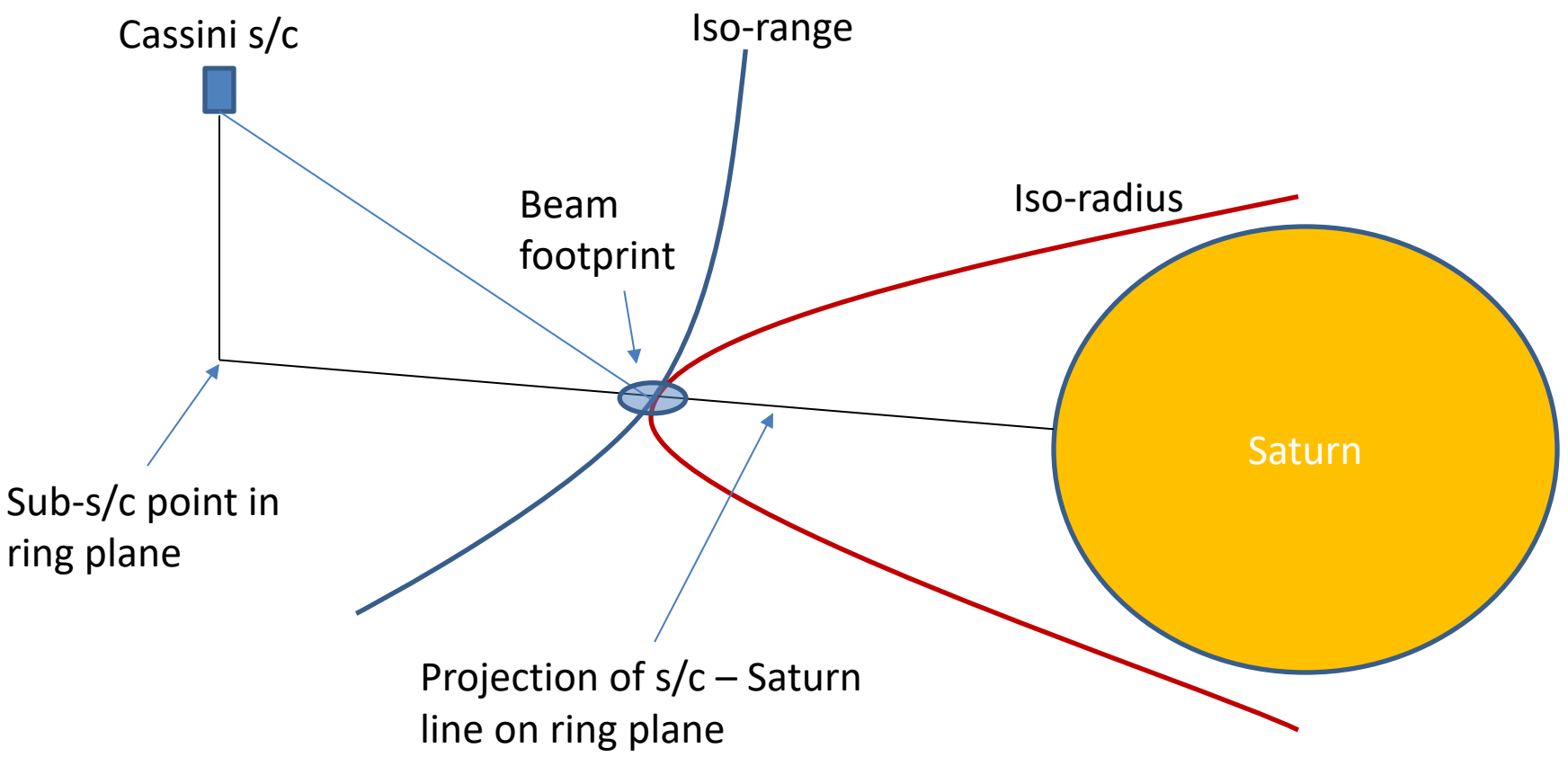

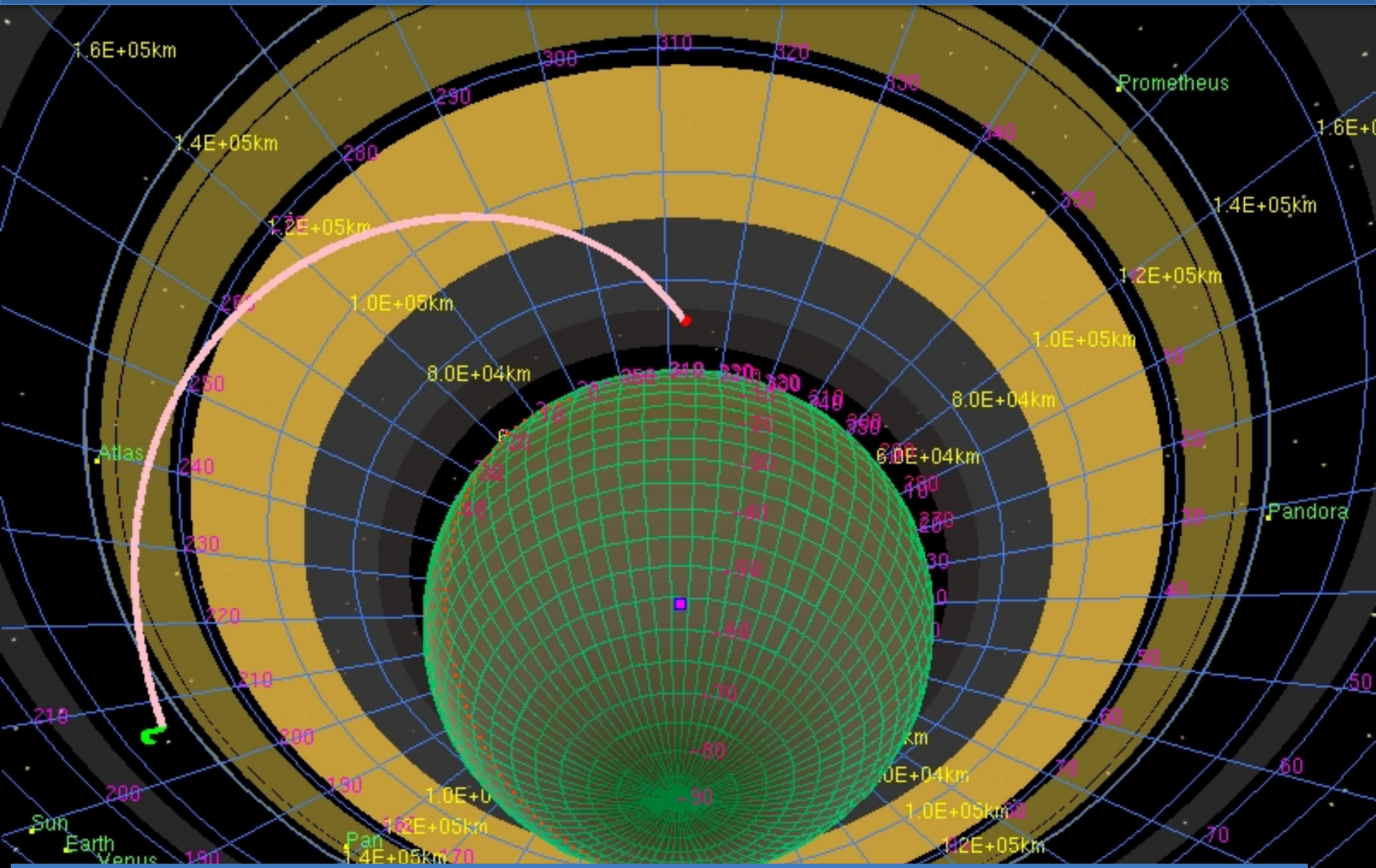
1.6E+05km
1.4E+05km
1.2E+05km
1.0E+05km
8.0E+04km
Prometheus
Atlas
Pandora
Sun
Earth
Venus
Pan

Ri_260

Calibrated Radar Backscatter From Rev 260 and Rev 282 Radar Ring Scans

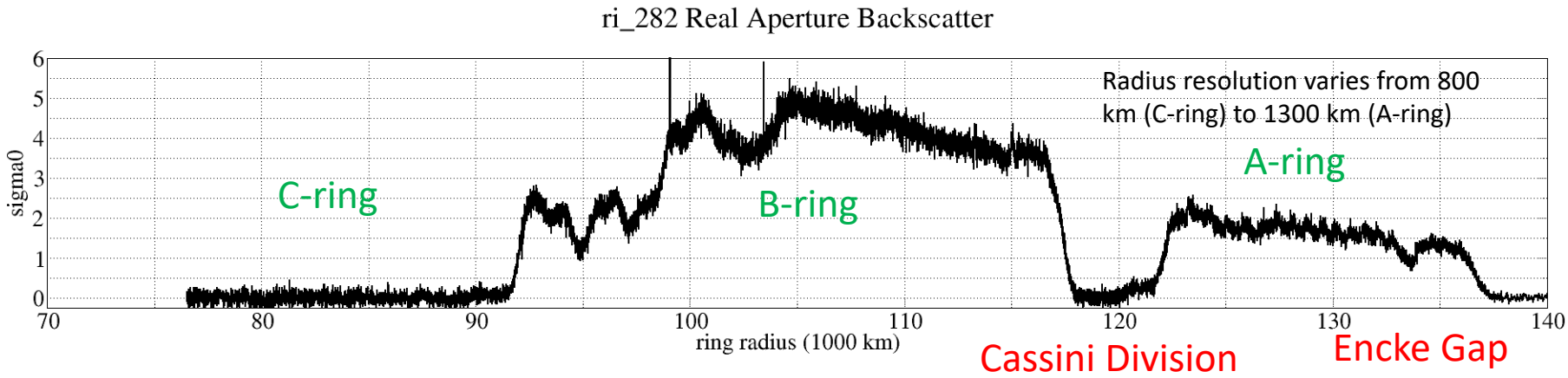

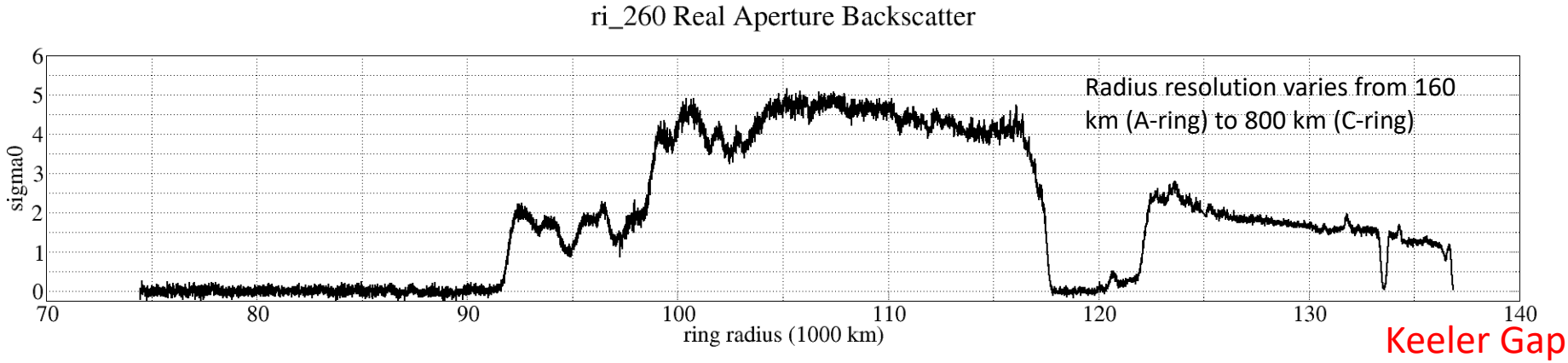

Note: sigma0 is normalized by area in the ring-plane and presented here in linear units. Unity sigma0 occurs when the received power equals what an isotropic scattering area would produce.

Expanded Views of Backscatter From Rev 260 and Rev 282 Radar Ring Scans

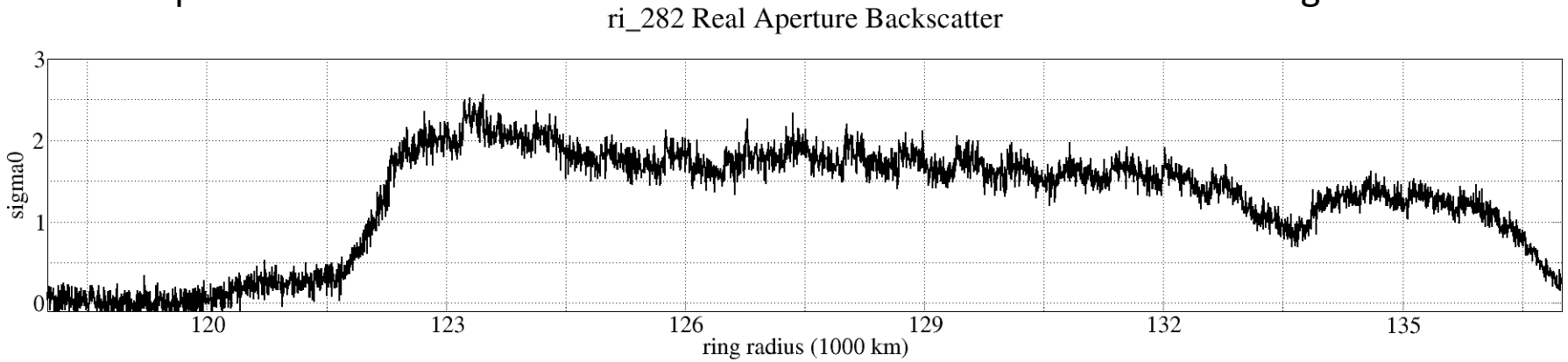

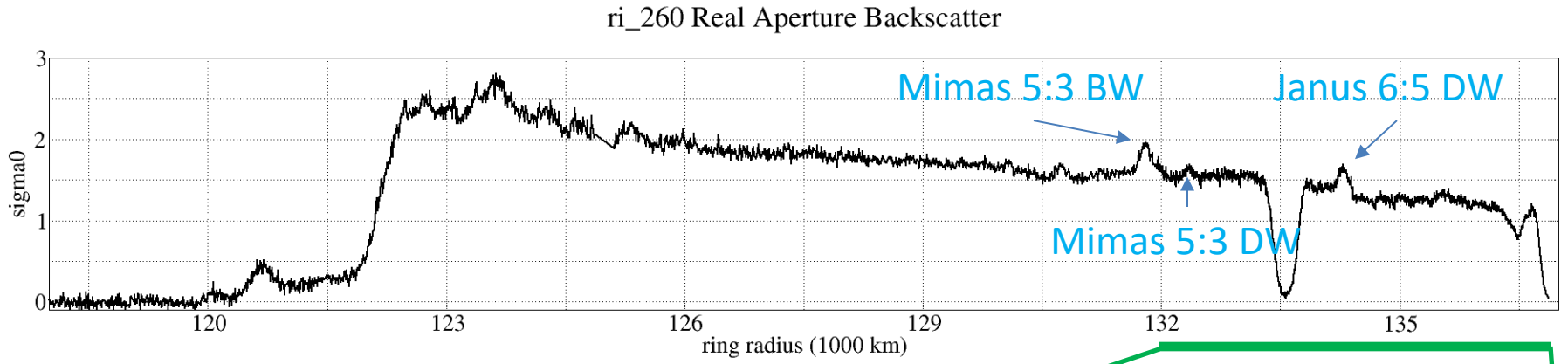

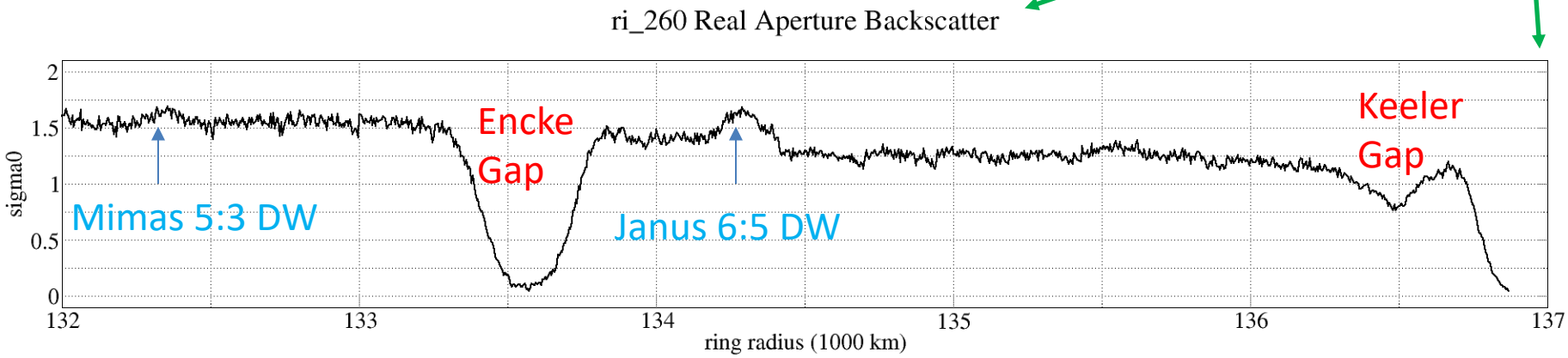

Real Aperture Summary

- Rapid variation of viewing geometry and radar parameters introduces some small-scale artifacts
- Consistent real aperture backscatter from ri_260 and ri_282
  - Incidence angle not important – volume scattering dominates
- Known ring features visible in radar data
- Ri_282 much lower resolution due to higher range
- Very high backscatter levels in A,B rings
  - Comparable to Xanadu on Titan and South polar region of Enceladus
  - Very low loss levels and complex dielectric structure at mm – cm scales.
  - Values > 3 hard to explain with existing scattering models

Comparison of Real Aperture and Range Compressed Backscatter

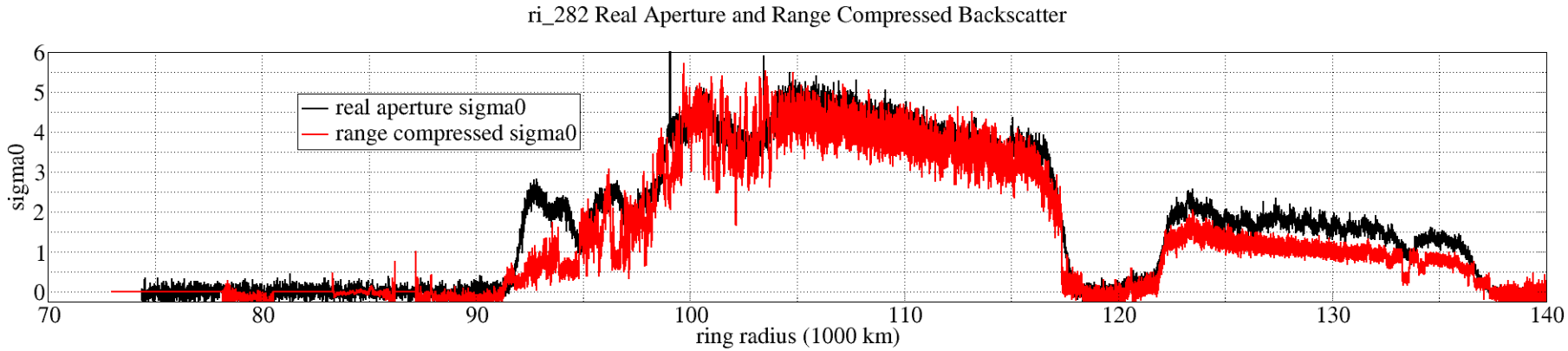

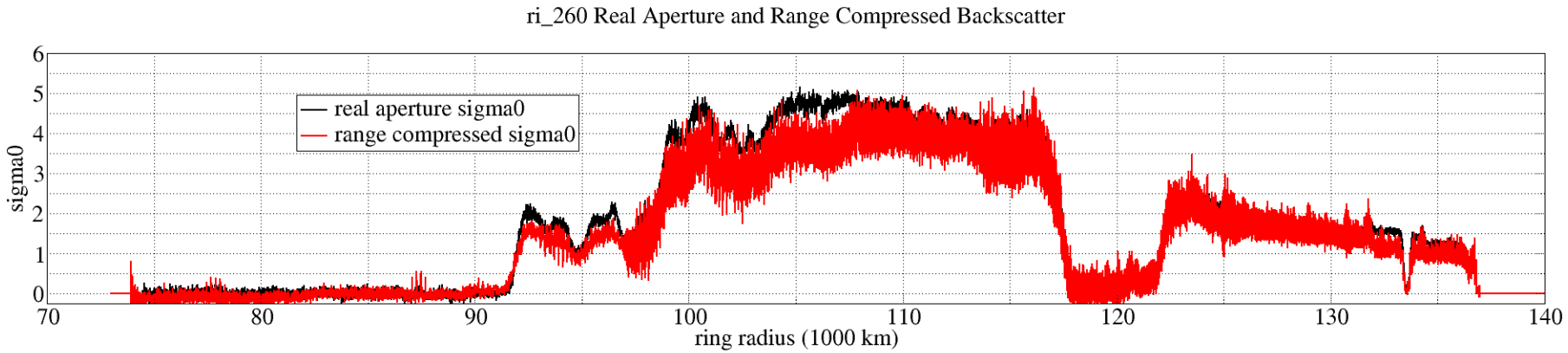

Detail of Ri_282 Backscatter in Ambiguity Free B-ring areas

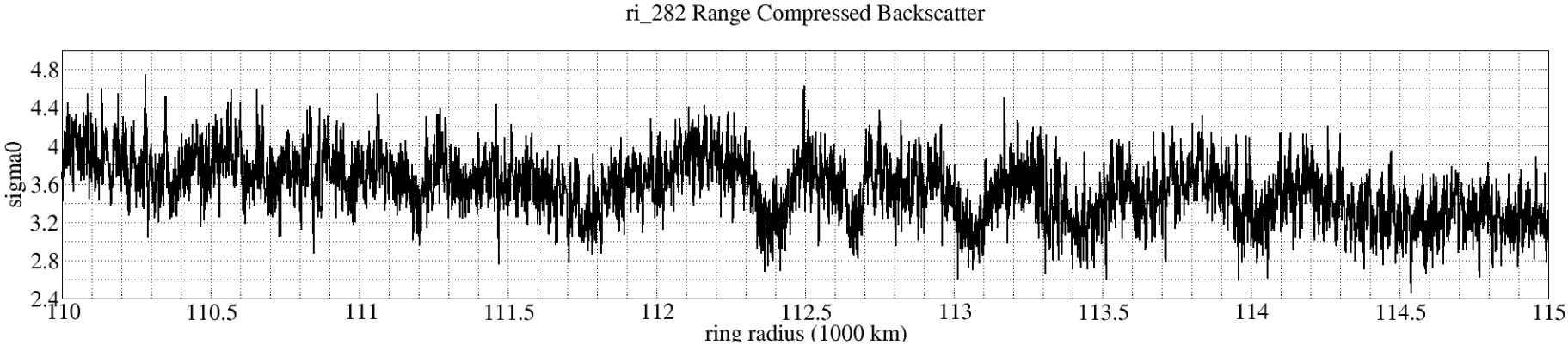

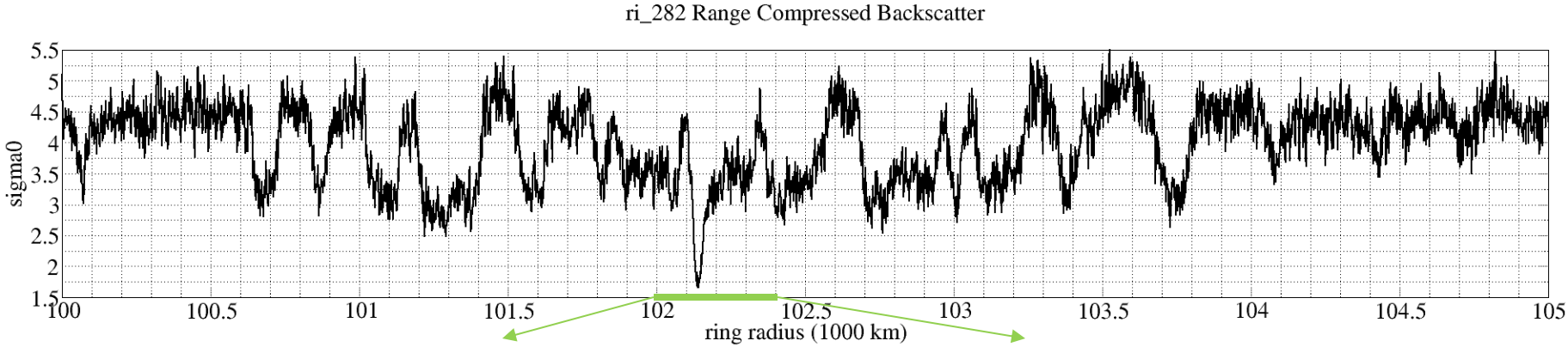

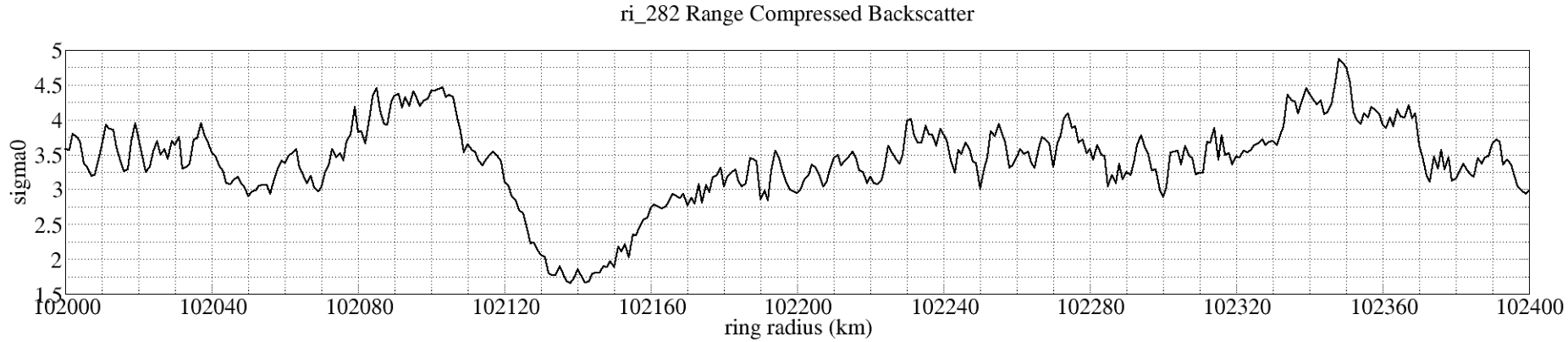

Range Compression Summary

- Range compressed calibrated backscatter matches real aperture results in general form. 0.5-1 dB scaling discrepancy.
- Consistent range compressed backscatter from ri_260 and ri_282
- Known ring features visible in radar data
- Ri_282 is ambiguity free in B,C-ring areas.
- Ri_260 has range ambiguities throughout – needs ambiguity correction procedure.
- Ambiguity correction procedure in progress

Earth Flyby Ground Track

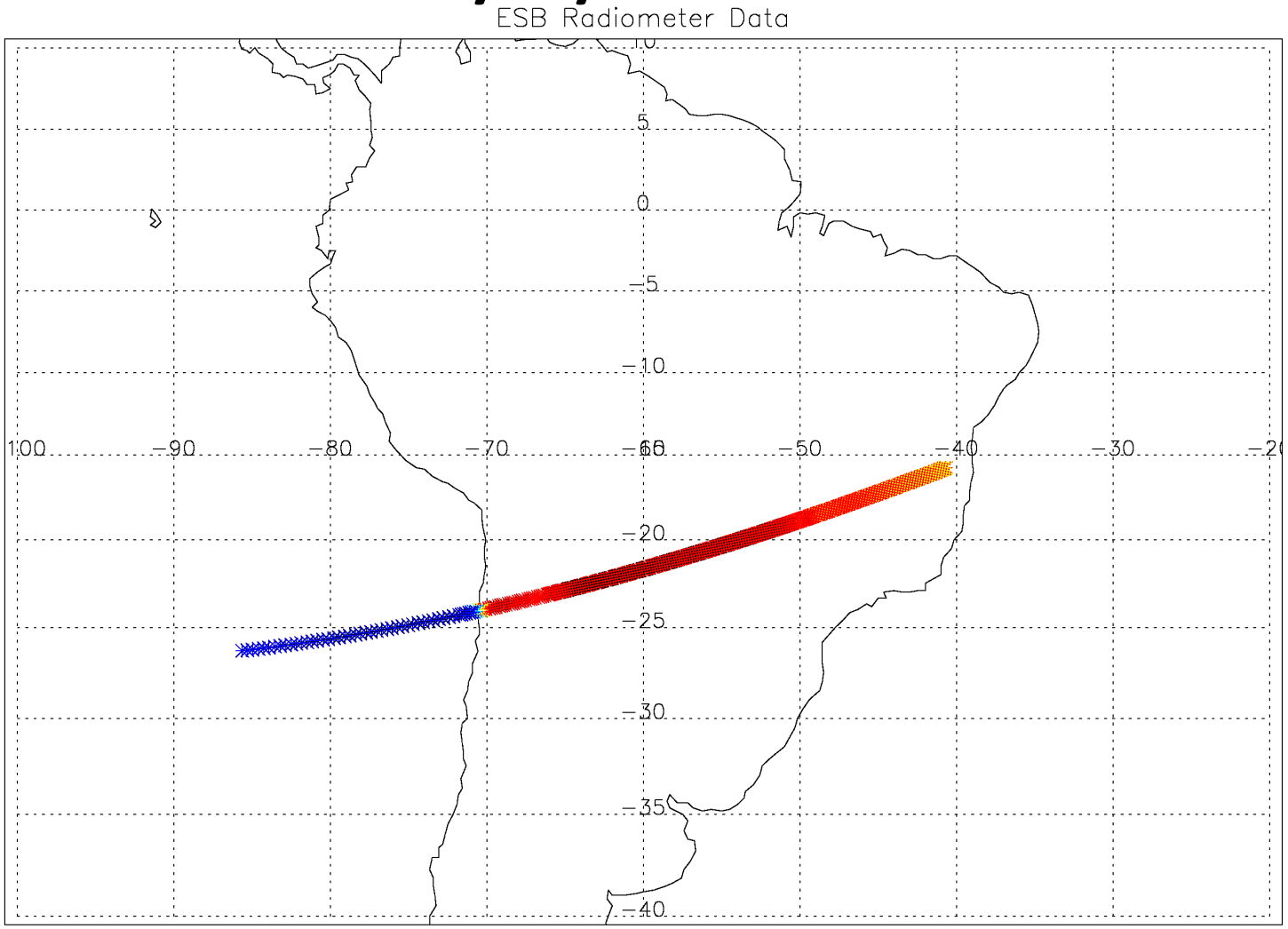

Absolute Calibration Validation

- Cassini and TRMM backscatter (both Ku-band) co-located in space, time, and incidence angle.
- Same calibration constants used on Cassini radar Earth flyby data as all other Cassini radar results
- Same processing code used on Earth Flyby and Rings (some differences in geometry routines – flat ring plane vs planetary surface).
- Noise floor computed based on engineering tests conducted during the Saturn Tour.
- Very good agreement on the absolute calibration.

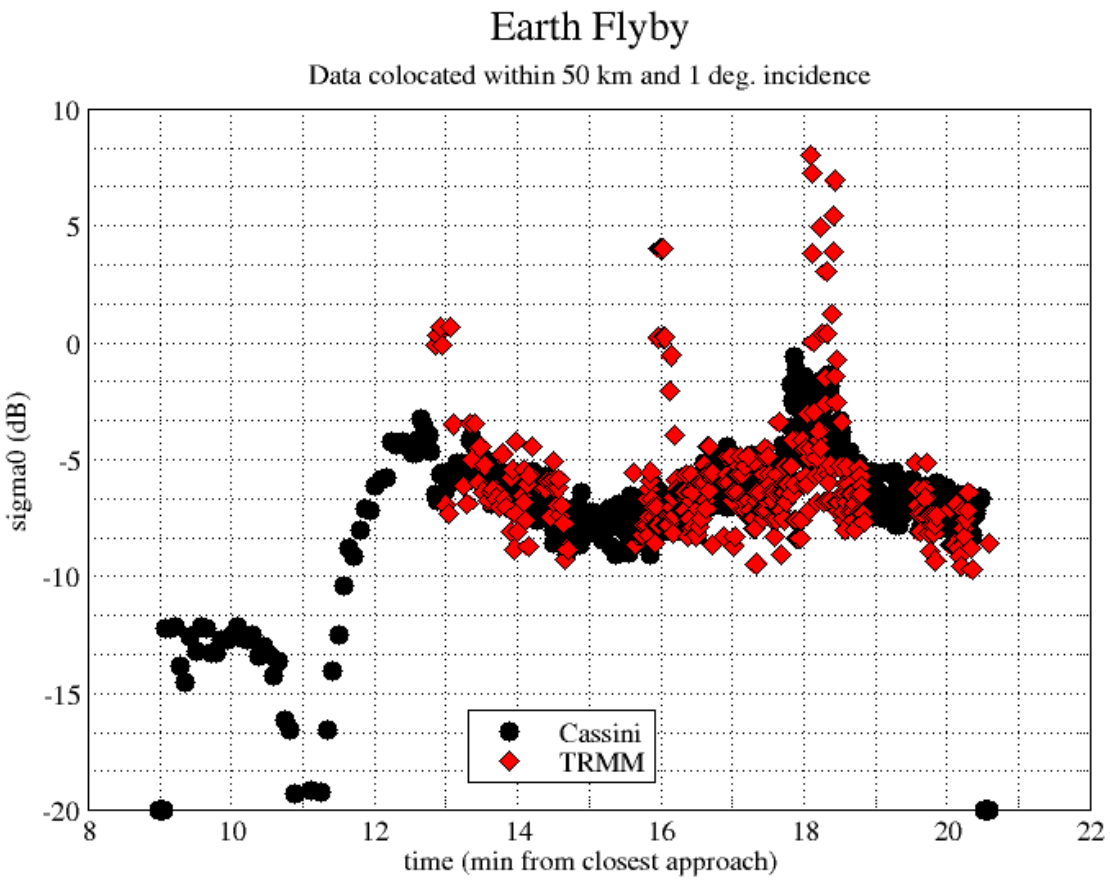

Earth Flyby Radiometry

- Cassini and TRMM brightness temperatures (both Ku-band) co-located in space, time.
- TRMM radiometer incidence angle is 49 deg. Vs Cassini incidence angles less than 20 deg. on land
- Cassini radiometer calibration based on engineering test results during Saturn Tour.
- Cassini polarization varies during flyby – close to V-pol over the ocean.

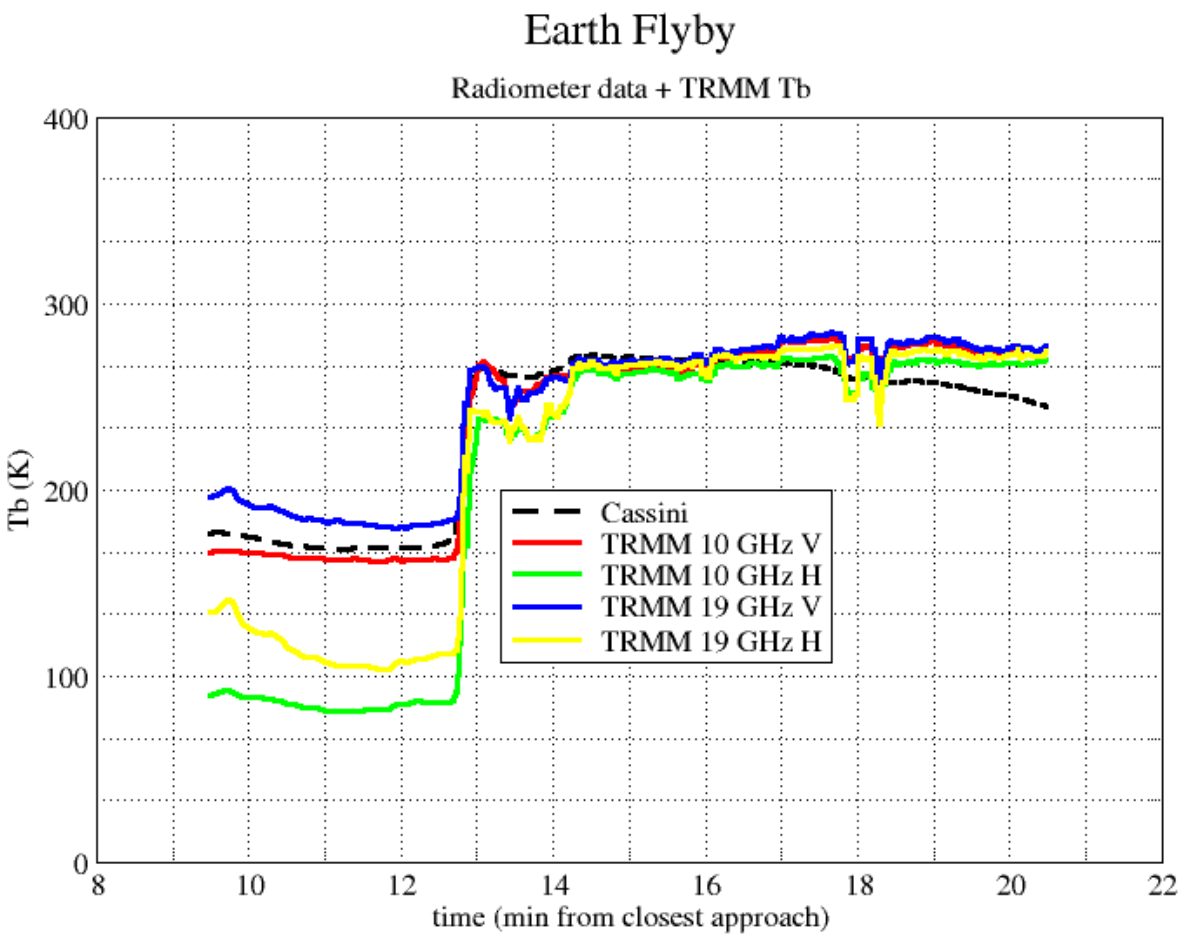

Validation Summary

- Earth Flyby allows comparison with separately calibrated Earth orbiting radar systems including TRMM which also operated at 13.8 GHz.
- Same calibration constants (ADC conversion, attenuator values, transmit power, receiver gain) applied to Earth flyby measurements and Saturn system measurements.
- Same processing code used on Earth flyby and Rings.
- Earth flyby measurements taken in 1999 (18 years before radar ring observations)
  - Engineering tests conducted during the Saturn Tour show very stable performance from the radar and radiometer.

- Backup

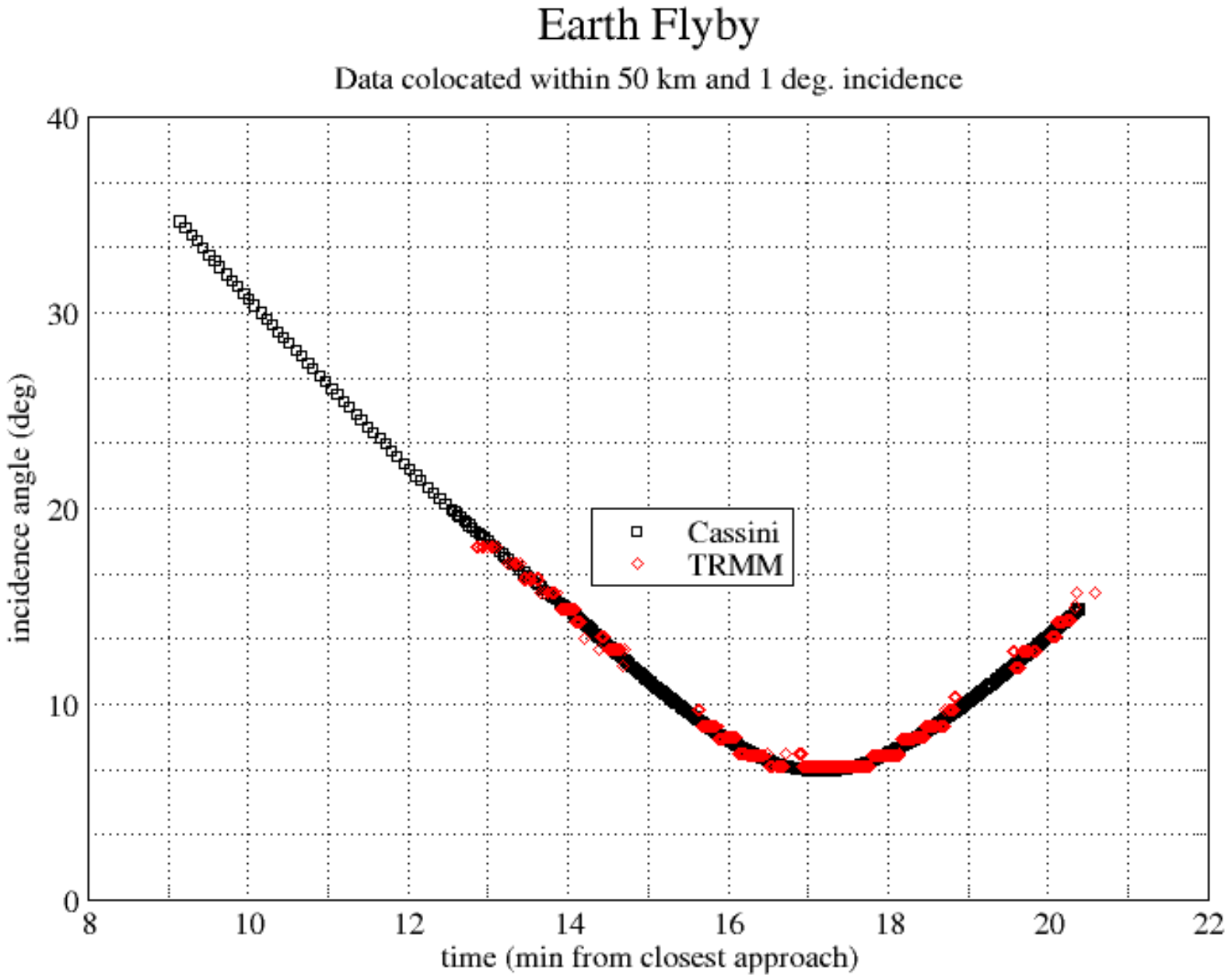
Earth Flyby
Data colocated within 50 km and 1 deg. incidence
incidence angle (deg)
time (min from closest approach)
Cassini
TRMM
0
10
20
30
40
8
10
12
14
16
18
20
22

Ground-Based Rings Backscatter

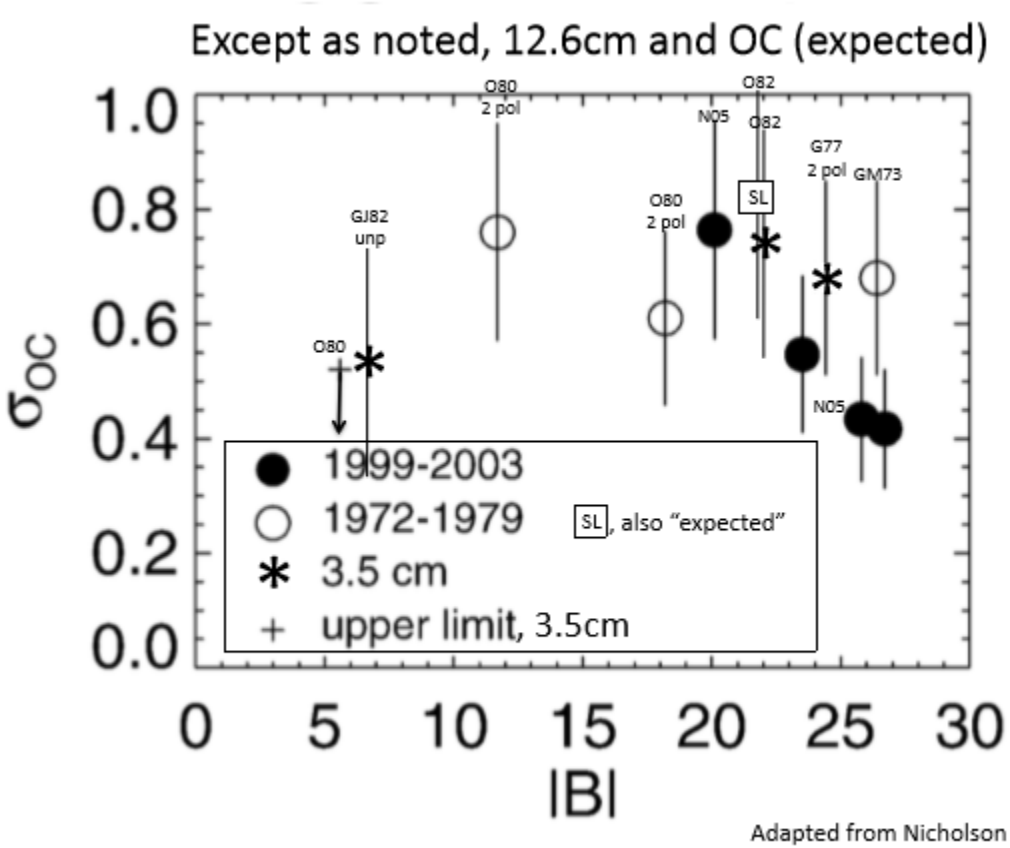

Adapted from Nicholson et al 2005

Figure2: Summary of "expected sense" single polarization radar reflectivity of the rings, σOC or σSL, for 3.5cm (asterisks) and 12.6cm (circles and square). Adapted from Nicholson et al 2005, Icarus.

The Rings of Saturn: Two-Frequency Radar Observations
R. M. GOLDSTEIN AND R. R. GREEN
Icarus 30, 1977

Observations of 3.5- and 12.6-cm radar echoes from the rings of Saturn suggest that no significant difference in scattering properties exists in this wavelength interval. The echoes are largely unpolarized at both wavelengths, and yield a radar cross section at 3.5 cm of 7.32 +- 0.84 X 10^9 km^2 for each polarization. The combined radar cross sections for both polarizations correspond to 1.37 +- 0.16 times the optically observed projected A- and B-ring areas (excluding that part of the rings shadowed by the planet). The shape of the echo spectrum is compatible with a homogeneous ring scattering model, except in having excess power at frequencies neat- the center of the spectrum. A number of possible explanations for the observed scattering properties are explored.

TABLE II

Geometry of Saturn's Rings[a]

Location	Radius (10^5 km)	Projected area for $B = -24°.4$[b] (10^9 km^2)	Corrected for occulted area (10^9 km^2)
Outer A	1.371		
		5.20	5.10
Inner A	1.216		
Outer B	1.167		
		6.83	5.98
Inner B	0.914		

[a] After Cook *et al.* (1973, Table IV).
[b] B is the angle between the line of sight and the plane of the rings.

Comparisons with Models

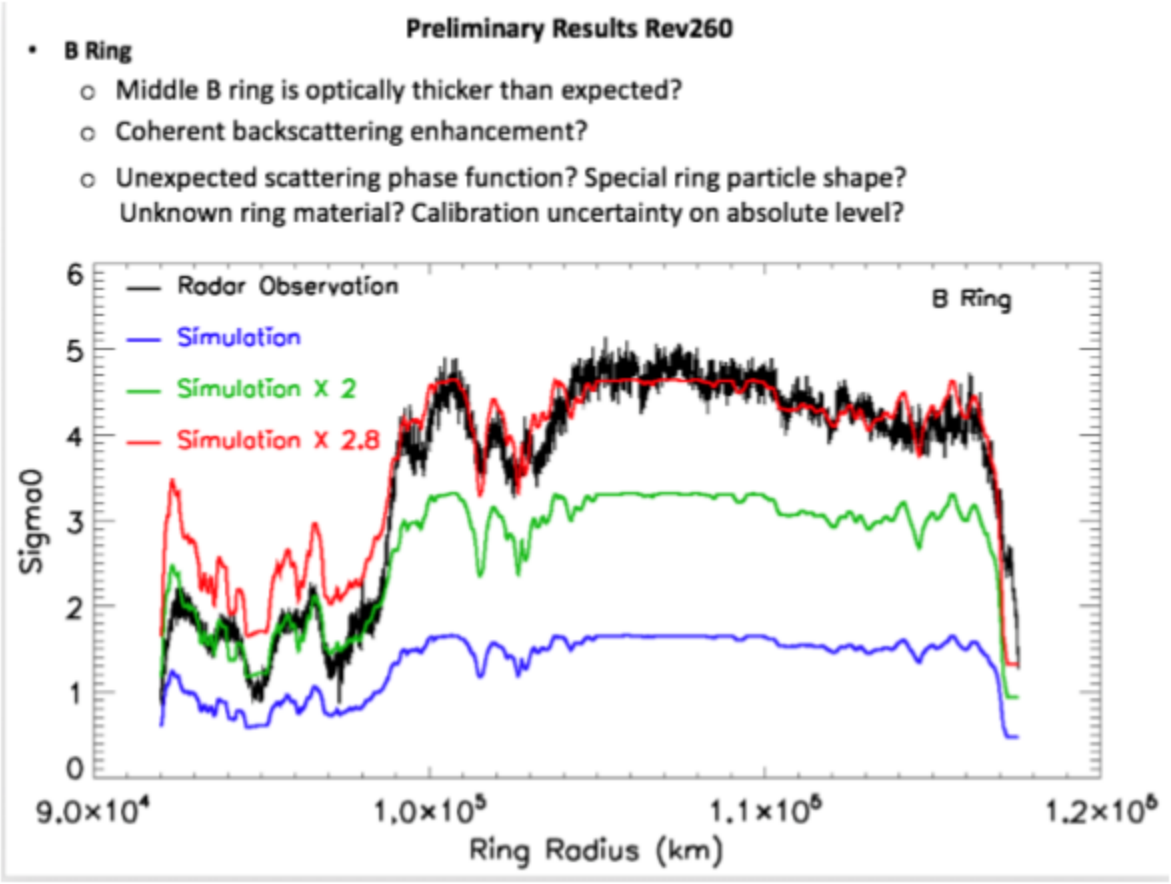

B Ring radar reflectivity, from January 2018 Radar Quarterly Report. Simulation results from Zhimeng Zhang.

Model Predictions

Predicted opening angle dependence of ring rada rreflectivity, curves. A and B show doubling code results with two different semi-empirical nonspherical particle models (from Cuzzi and Pollack 1978).

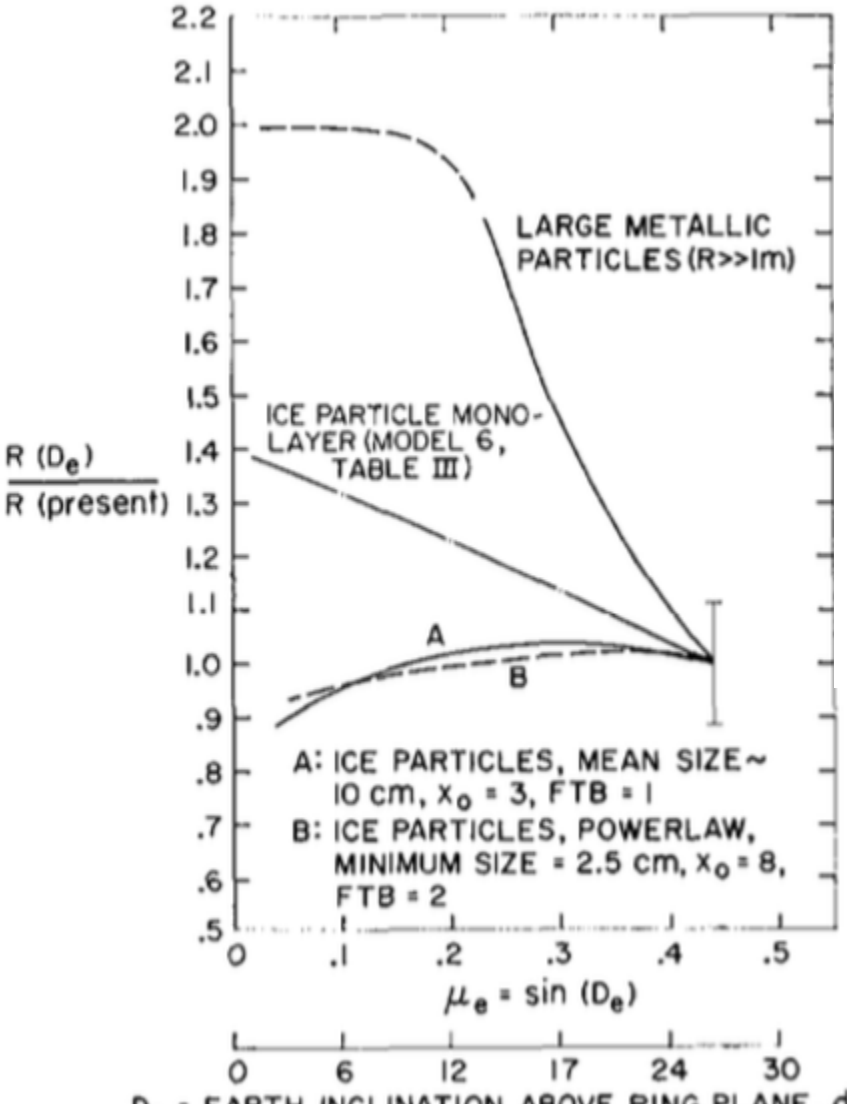

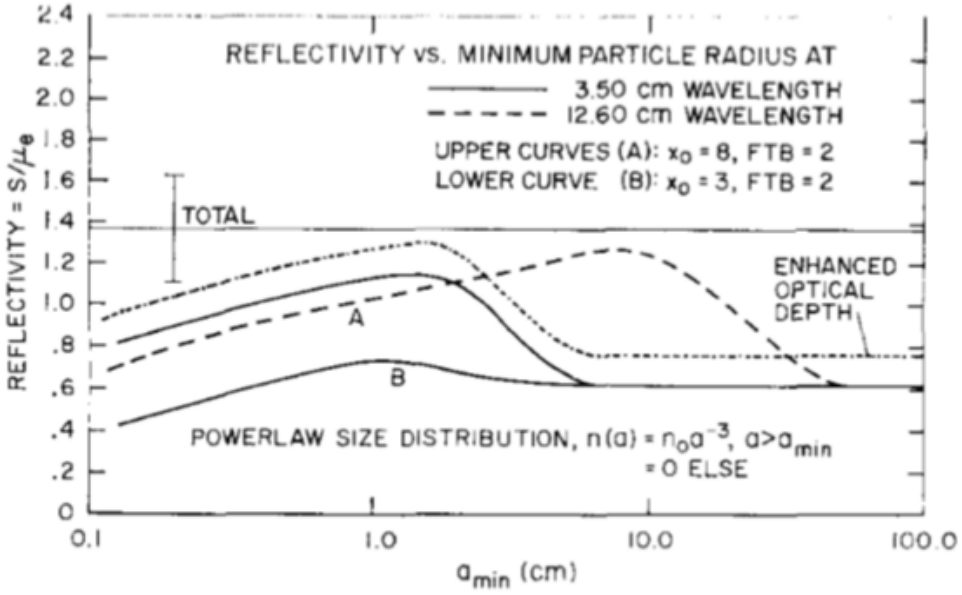

Model total radar cross section (both polarizations) at 3.5 and 12.6cm wavelength, for power law size distributions of different minimum size, and different nonspherical particle parameters (from Cuzzi and Pollack 1978).

Ambiguity Correction

- Correlated signal power for a given radius (time delay) is the sum of echoes from a set of ambiguous radii separated by integer PRI interval and speckle noise
- $P_s(i) = n_s + 1/N_p \Sigma_j X(i,k)\sigma_0(j,k)$
  - burst i, pulse j, radius bin k
- Average over pulses in a burst to reduce speckle noise n_s
- Form over-determined linear system where each burst provides one equation from different parts of the antenna pattern
  - $[<P_s>] = [[X]] [\sigma_0]$
- Apply singular value decomposition to solve for the $[\sigma_0]$ in least squares sense
- Algorithm needs detailed tuning with spatial (ie., radial) averaging used to reduce noise.

Comparison of Averaged Real Aperture and Range Compressed Backscatter

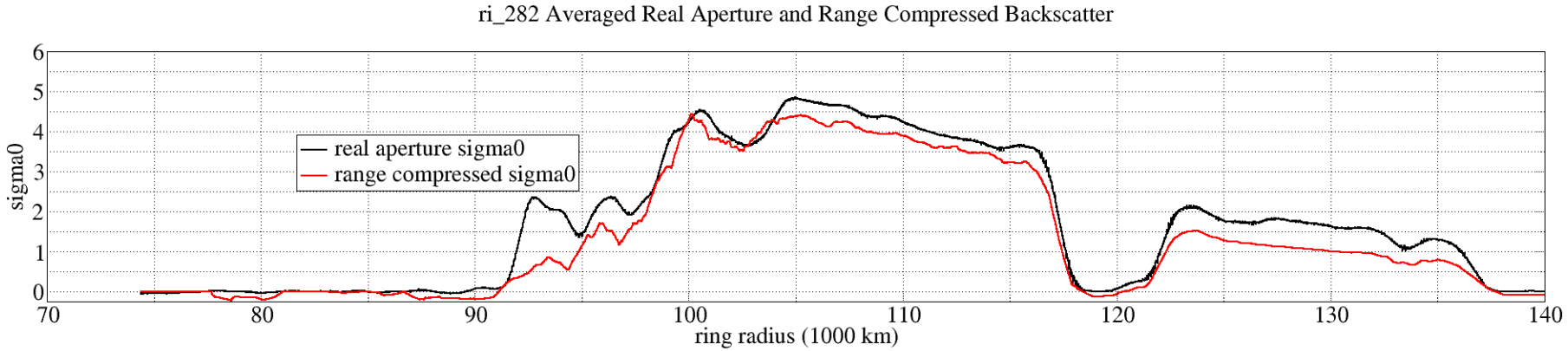

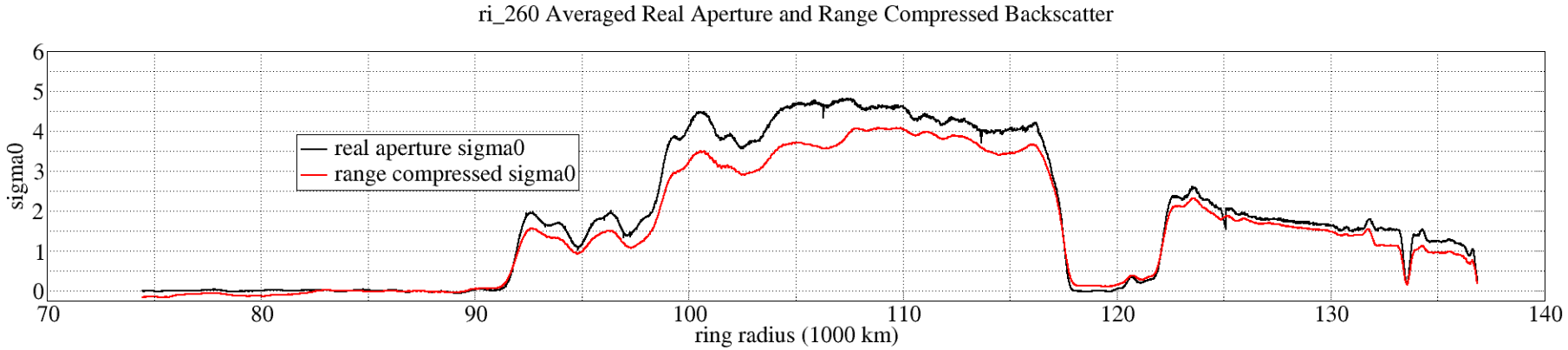

Averaging taken over the radius extent of the beam footprint.

Range Compression

- Time domain correlation process applied to each pulse echo which illuminates a given radius bin
- Ambiguity locations (in radius) determined for each burst and included in numerical integration of the range resolution cell area
  - Needed for proper scaling to backscatter, even if no ambiguity correction is applied.
- Noise Subtraction applied using same noise level as real aperture processing.
- Scaling from data counts to power in Watts and then to backscatter uses the same parameters as for real aperture processing.
  - Numerical integrations required for accuracy
  - Radar equation numerical integrations are taken over the primary and ambiguity range bin areas rather than the whole beam main lobe footprint.

Range Compressed Backscatter

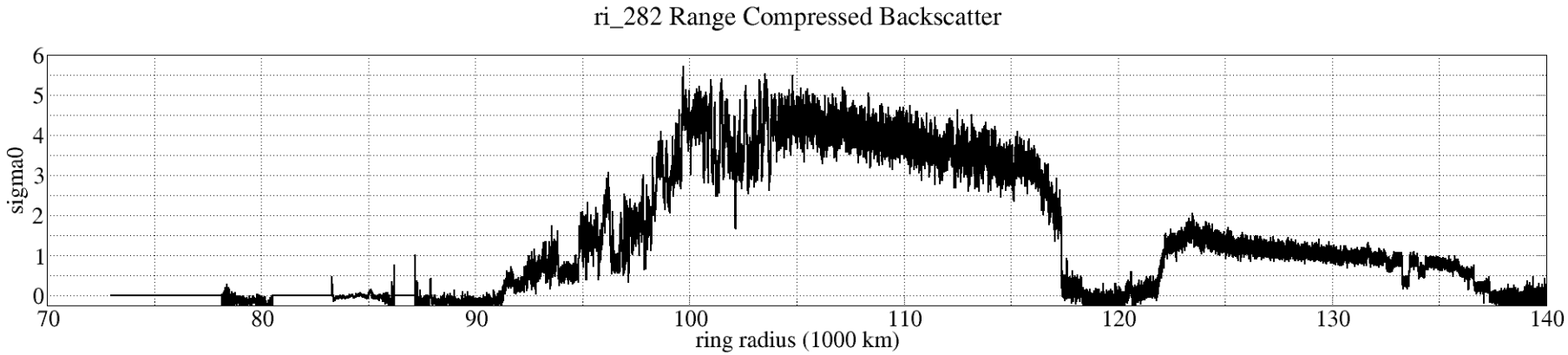

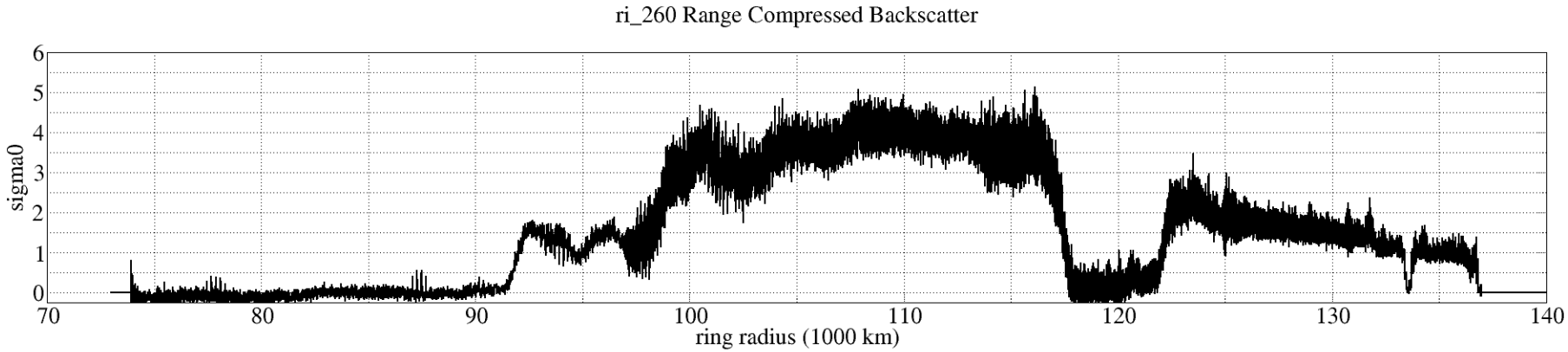

Uncalibrated Raw Powers From Rev 260 and Rev 282 Radar Ring Scans

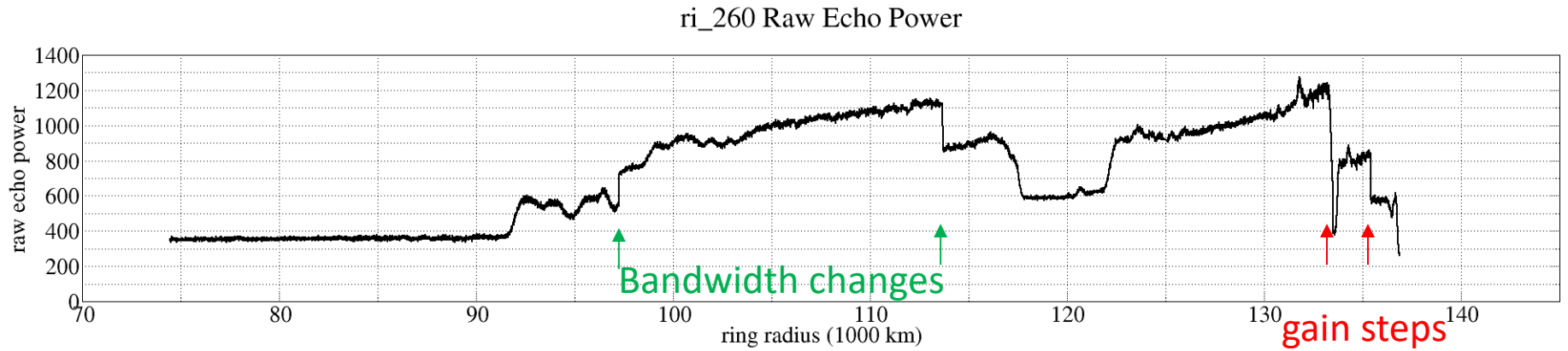

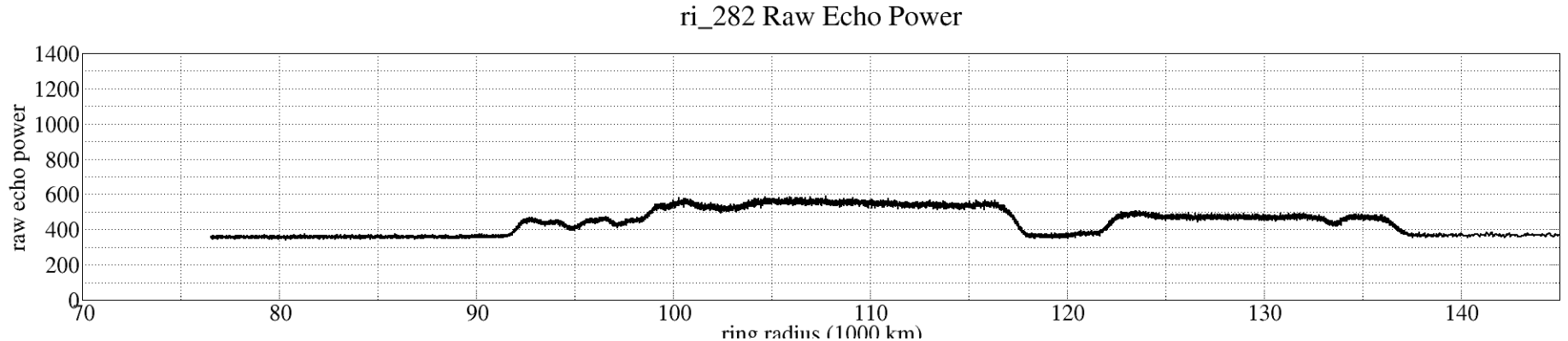

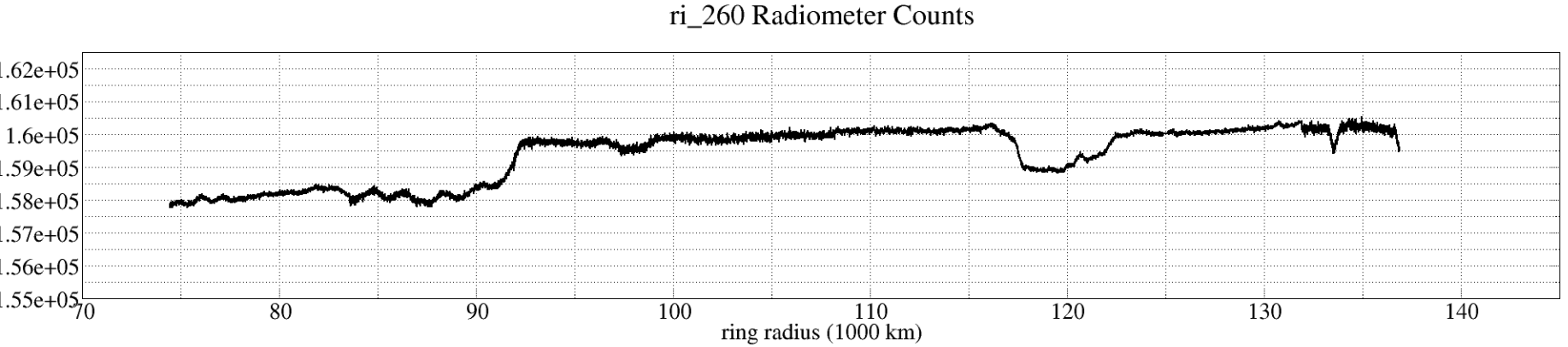

Scaling Raw Powers to Normalized Backscatter

- Raw echo power in data counts
  - $V_{sn} = 1/N_{rw} \Sigma |v(i)|^2$
- Noise Subtraction
  - $V_s = V_{sn} - V_n$
- Scaling from data counts to power in Watts
  - $P_s = C V_s \quad P_n = C V_n = kT_{sys}B_{rcv}$
  - C is a calibration conversion constant which depends on the attenuator setting and bandwidth mode.
- Radar Equation relates received power to normalized backscatter cross-section σ_0
  - $P_s = \lambda^2/(4\pi)^3 \int P_t u_{rw} G^2 \sigma_0 / R^4 \, dA$

Radar Equation Details

- Rapid variation of viewing geometry and radar parameters requires detailed duty cycle correction to obtain accurate real aperture results.
- $P_s = \lambda^2/(4\pi)^3 \, P_{t0}\sigma_0/R^4 \int 1/N_{rw}\Sigma\Sigma p(t - i\tau_{pri}-2R/c) \, u_{rw}(t) \, G^2 \, dA$
- $p(t) = 1$ for $0 < \tau < \tau_p$, 0 otherwise
- $u_{rw}(t) = 1$ for $\tau_{rwd} < \tau < \tau_{rwd} + \tau_{rw}$, 0 otherwise

Observing Geometry

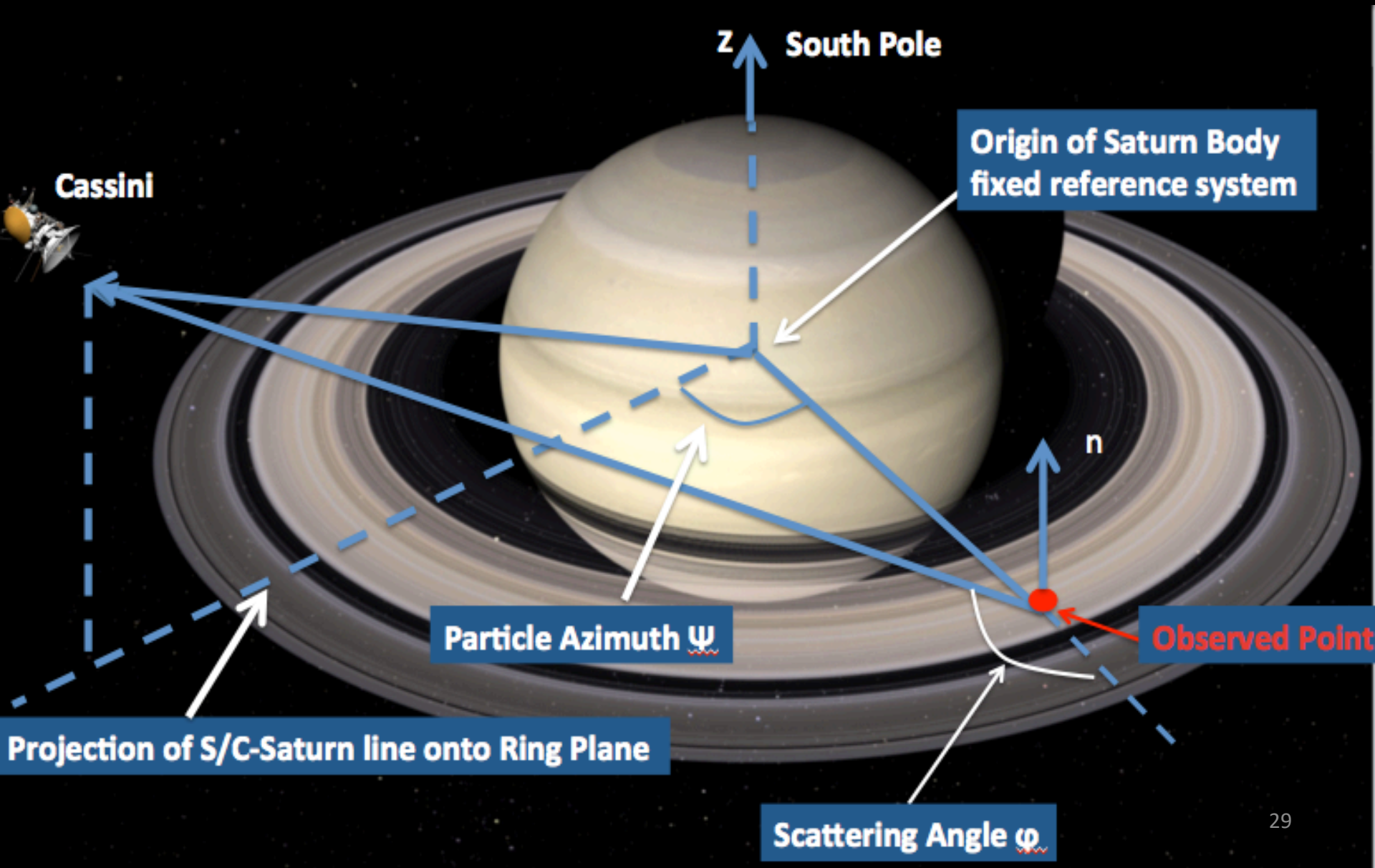

1-D Range Slicing

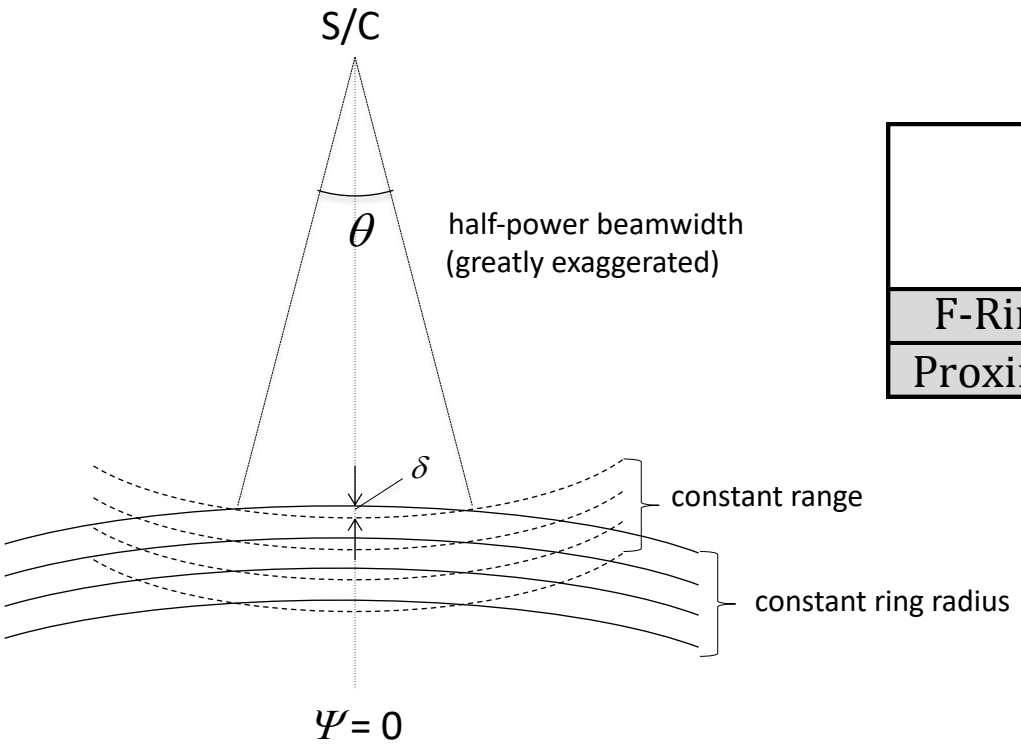

Geometric Smearing

δ	Inner C Ring [m]	Outer A Ring [m]
F-Ring Orbit	500	75
Proximal orbit	80	450

Observing point centered at zero azimuth angle relative to spacecraft